THE JOURNAL OF PHYSICAL CHEMISTRY A

Article

pubs.acs.org/JPCA

Substituent and Solvent Effects on the UV−vis Absorption Spectrum of the Photoactive Yellow Protein Chromophore

F. Fernández García-Prieto,[†] M. A. Aguilar,*[,†] I. Fdez. Galván,[‡] A. Muñoz-Losa,[†] F. J. Olivares del Valle,[†] M. L. Sánchez,[†] and M. E. Martín*[,†]

[†]Área de Química Física, University of Extremadura, Avda. Elvas s/n, José M.a Viguera Lobo Building, 06071 Badajoz, Spain

[‡]Department of Chemistry−Ångström, The Theoretical Chemistry Programme, Uppsala University, P.O. Box 518, SE-751 20 Uppsala, Sweden

Supporting Information

ABSTRACT: Solvent effects on the UV−vis absorption spectra and molecular properties of four models of the photoactive yellow protein (PYP) chromophore have been studied with ASEP/MD, a sequential quantum mechanics/molecular mechanics method. The anionic *trans-p*-coumaric acid (pCA$^-$), thioacid (pCTA$^-$), methyl ester (pCMe$^-$), and methyl thioester (pCTMe$^-$) derivatives have been studied in gas phase and in water solution. We analyze the modifications introduced by the substitution of sulfur by oxygen atoms and hydrogen by methyl in the coumaryl tail. We have found some differences in the absorption spectra of oxy and thio derivatives that could shed light on the different photoisomerization paths followed by these compounds. In solution, the spectrum substantially changes with respect to that obtained in the gas phase. The n → π_1* state is destabilized by a polar solvent like water, and it becomes the third excited state in solution displaying an important blue shift. Now, the $\pi \rightarrow \pi_1$* and $\pi \rightarrow \pi_2$* states mix, and we find contributions from both transitions in S1 and S2. The presence of the sulfur atom modulates the solvent effect and the first two excited states become practically degenerate for pCA$^-$ and pCMe$^-$ but moderately well-separated for pCTA$^-$ and pCTMe$^-$.

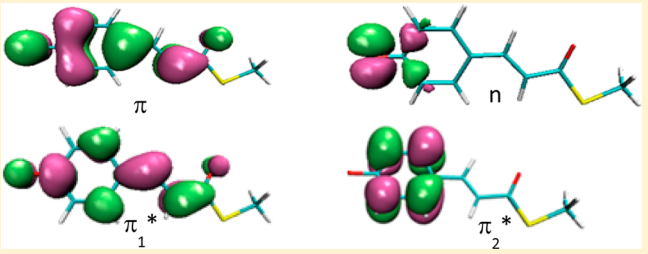

INTRODUCTION

Photoisomerization reactions have been profusely studied as they play an important role in biological processes such as vision, energy production, signaling, etc.[1−3] Moreover, understanding how nature drives those processes is a necessary tool for the development of biotechnological devices. The comprehension of such mechanisms needs the complementary effort of experimental and theoretical studies of the chromophore in different environments: gas phase, solution, and inside the protein.

The photoactive yellow protein (PYP), originally discovered in the *Halorhodospira halophile* bacterium,[4,5] is responsible for its negative phototaxis when irradiated with blue light.[6] Nowadays, it is accepted that the final cellular response is initiated with the photoisomerization of the PYP chromophore, the deprotonated 4-hydroxy-cinnamic acid (or anionic *trans-p*-coumaric acid, pCA$^-$) bonded to the γ-sulfur of Cys62 through a thioester linkage.[7] After irradiation (446 nm), the protein enters a photocycle where the primary event is the isomerization of the chromophore's double bond[8−11] on a subpicosecond timescale, very similar to retinal photoisomerization in the visual process.[1]

PYP shows an absorption maximum at 446 nm, which is very close to the absorption of its isolated chromophore (≈430 nm). This fact has also been reported in other proteins and chromophores.[12] Nowadays, it is accepted that inside the protein, the chromophore is exposed to numerous interactions that all together render the absorption practically unchanged with respect to the gas phase values. In a recent paper, Rajput et al.,[13] by performing gas phase absorption measurements on pCA$^-$ and pCA$^-$ $(H_2O)_2$, reported the effect exerted by the H bonds on the spectrum. Two water molecules simulate the interaction of the phenolic end of the chromophore with the amino acid residues Glu46 and Tyr42 present in the protein. They found an 85 nm (0.71 eV) blue shift associated with the hydrogen bond interaction. Other factors present inside the protein, like electrostatic environment or geometrical constraints, would red shift the absorption maximum counteracting the H bonds effect and yielding the absorption unchanged. The protein environment protects the chromophore from the surrounding solvent, avoiding the blue shift that would be expected. A deeper knowledge about the chromophore−solvent interactions would be extremely useful to the understanding of the effect exerted by the protein environment.

In the literature, there exist a vast number of experimental studies about the absorption spectrum and excited state

Special Issue: Jacopo Tomasi Festschrift

Received: February 11, 2015
Revised: April 21, 2015
Published: April 24, 2015

DOI: 10.1021/acs.jpca.5b01434
J. Phys. Chem. A 2015, 119, 5504−5514

deactivation of several derivatives of the anionic *trans-p*-coumaric acid.[14−18] Most of them in solution and just a few in gas phase.[19] These studies point out the importance of the protonation state of the chromophore together with the nature of its coumaryl tail on the kinetic and thermodynamic product of the photoisomerization. For instance, it has been shown that pCA^{2-} (*trans-p*-hydroxycinnamate) and $pCMe^-$ (*trans-p*-hydroxycinnamide) exhibit a decay of the excited-state bands of 10 and 4 ps, respectively, and a net *trans* to *cis* isomerization is recorded.[20,21] On the contrary, pCT^- (*trans-p*-hydroxythiophenyl cinnamate) decays in less than 2 ps and no *cis* product has been found.[20,21] From the theoretical side, *trans-p*-coumaric acid derivatives have also been profusely studied, both in gas phase[22−24] and in solution. When the environmental effects are taken into account, different strategies can be followed. From the simplest consideration of a few solvent molecules[25−27] strategically introduced in order to mimic the main interactions with the medium to the most sophisticated QM/MM methods,[29,30] as for instance the ASEP/MD method.[31,32,37] In between, the explicit quantum introduction of the closest protein residues[28] or the representation of the environment as a continuum[33] have also been employed.

In this article, we have mainly focused on the analysis of the water effect and coumaryl tail of the monoanionic *trans-p*-coumaric chromophore during the very first event after the irradiation with blue light. To this end, the first two electronic transitions for the acid (pCA^-), thioacid ($pCTA^-$), methyl ester ($pCMe^-$), and methyl thioester ($pCTMe^-$) derivatives have been studied in gas phase and in water solution. The methyl thioester explores the role of the thioester linkage, present in the PYP protein. We will analyze the modifications introduced by the substitution of sulfur by oxygen atoms with the $pCMe^-$ derivative. pCA^- and $pCTA^-$ permit the evaluation of the influence of the methyl group. We tried to analyze if already during the absorption process it could be possible to find some differential characteristic that could explain the different deactivation path experimentally found for pCT^- in solution.

In a previous paper,[32] we analyzed the effects of the solvent and protonation state on the electronic absorption spectrum of the *p*-coumaric acid. The calculated solvatochromic shift of the absorption maximum is a red shift for the neutral, carboxylate monoanion, and dianionic chromophores and a blue shift for the phenolate monoanion. We also analyzed the contribution of the solvent electronic polarizability on the solvent shift. It was concluded that it represents an important part of the total solvent shift for the neutral form, but its contribution was completely negligible in the mono- and dianionic forms. This difference is related to the different nature of the solute−solvent interactions. So, while in neutral species, the interaction is dominated by the solute dipole−solvent reaction field term, in anionic compounds the main contribution comes from the interaction between the charge of the solute and the solvent reaction potential. The reaction electric field is increased by the electronic solvent polarization, but it hardly affects the electrostatic potential value. Consequently, the electronic solvent polarization term has not been included in the present study where only monoanionic species are considered.

METHOD

Solvent effects on the absorption spectra and molecular properties of four models of the PYP protein chromophore were studied with the ASEP/MD (averaged solvent electrostatic potential from molecular dynamics) method. This is a sequential quantum mechanics/molecular mechanics method (QM/MM) that makes use of the mean field approximation (MFA).[31,34,35] In this approximation, instead of considering specific solvent configurations, the perturbation enters into the solute molecular Hamiltonian in an averaged way. Consequently, ASEP/MD through the MFA permits the reduction of the number of quantum calculation from several thousands, as usual in QM/MM[36] methods, to only a few, and the highest levels of theory available at present can be employed. Other sequential QM/MM methods using the MFA are RISM/SCF,[42−44] ASEC/MC,[45] MF-QM/MM,[46] and methods based in the frozen density embedding theory (FDET).[47] The main difference between them is the way in which the averaged representation of the solvent is obtained and introduced in the QM calculations.

From the two components into which the solvent response is traditionally split, inertial (associated with nuclear movements) and electronic (associated with the response of the electronic degrees of freedom of the solvent), the latter is considered fast enough to be always in equilibrium with the solute charge distribution. On the contrary, nuclear movements are slower than electronic ones and longer times are needed in order to reach equilibrium. In this context, during a Franck−Condon (FC) transition, the change in the solute charge distribution is supposed as so fast that the inertial component of the solvent will be in a nonequilibrium situation with the final state (i.e., the solvent structure around the initial state remains fixed during the transition). Consequently, the first step in the study of vertical transitions in solution always consists in the determination of the solvent structure in equilibrium with the solute geometry and charge distribution in the starting state, the ground state if we deal with absorptions. To this end, we used the ASEP/MD methodology where quantum calculations and molecular dynamics simulations are engaged in the context of the MFA.[38] That is, from a fully MM molecular dynamics simulation[39] an averaged solvent electrostatic potential is obtained, and it is introduced as a point-charge representation into the quantum calculation of the solute. Once the associated Schrödinger equation has been solved, the updated solute charge distribution is used in a new molecular dynamics simulation. MM simulations and quantum calculations are successively iterated until the charge distribution of the solute and the solvent structure around it become mutually equilibrated. The point charges representing the solute molecule during the MD simulation are obtained from the in solution solute molecule wave function by using the CHELPG (charges from electrostatic potential, grid) method.[40,41]

As the ASEP/MD method has been described in previous papers,[31,32] here we just present a brief outline. As in other QM/MM methods, the solute wave function is obtained by solving the effective Schrödinger equation

$$(\hat{H}_{QM} + \hat{H}^{elect}_{QM/MM} + \hat{H}^{vdw}_{QM/MM})|\Psi\rangle = E|\Psi\rangle \quad (1)$$

$\hat{H}_{QM}$ is the in vacuo solute molecular Hamiltonian and the electrostatic solute−solvent interaction term ($\hat{H}^{elect}_{QM/MM}$) is calculated using the mean field approximation

$$\hat{H}^{elect}_{QM/MM} = \int d\mathbf{r}\cdot\hat{\rho}\cdot V_{ASEP}(r) \quad (2)$$

$V_{ASEP}(r)$ is the average electrostatic potential generated by the solvent in the volume occupied by the solute, and it is

DOI: 10.1021/acs.jpca.5b01434
J. Phys. Chem. A 2015, 119, 5504−5514

represented through a set of point charges. Technical details about the determination of the number, position, and values of the charges can be found in ref 31. $V_{ASEP}(r)$ is calculated as a statistical average over the configuration space obtained in the MD simulations. Finally, $\hat{\rho}$ is the charge density operator of the solute and $\hat{H}^{vdw}_{QM/MM}$ is the Hamiltonian for the van der Waals interaction. When represented through a Lennard-Jones potential, this term is a function of the nuclear coordinates and it does not depend on the electron coordinates.

Given that $V_{ASEP}(r)$ and ρ, the solute charge density, depend mutually each on the other, eqs 1−2 must be solved iteratively. The process finishes when convergence in the solute charge distribution and energy is reached.

The ASEP/MD process can be extended by carrying out the relaxation of the solute geometry during the quantum calculation. The method optimizes the solute geometry in the presence of the solvent using a technique described in a previous paper[48] and based on the joint use of the free-energy gradient method[49−52] and the mean field approximation. At each step of the optimization procedure, the mean values of the total force (F) and, when possible, the Hessian (H) are calculated from a representative set of solvent configurations and then used to obtain a new geometry with the rational function optimization method.

Once the optimization is finished, the geometry and charge distribution of the solute and the solvent structure become mutually equilibrated. When one is interested in studying electronic transitions, it could be interesting to perform an additional self-consistent process during the calculation of the ASEP. The solvent structure (the set of solute−solvent configurations in equilibrium) and solute geometry obtained in the first self-consistent process are used to couple the quantum mechanical solute and the electron polarization of the solvent. In a previous paper,[32] we showed that solvent electronic polarizability has a very small effect on the transition energies of the anionic *p*-coumaric acid. Consequently, and in order to simplify calculations, we neglect the effect of this component along this paper. In sum, the variation of the chromophore absorption energy when it passes from gas phase to solution, known as solvent shift, can be written as

$$\delta = \langle \Psi | \hat{H}_{QM} + \hat{H}^{elect}_{QM/MM} + \hat{H}^{vdw}_{QM/MM} | \Psi \rangle - \langle \Psi^0 | \hat{H}_{QM} | \Psi^0 \rangle \quad (3)$$

$$\delta = \langle \Psi | \hat{H}_{QM} | \Psi \rangle - \langle \Psi^0 | \hat{H}_{QM} | \Psi^0 \rangle + \langle \Psi | \hat{H}_{\frac{elect}{QM/MM}} | \Psi \rangle + E^{vdw}_{QM/MM} \quad (4)$$

$$\delta = E_{dist} + E_{int} = E_{dist} + E^{elect}_{int} + E^{vdw}_{int} \quad (5)$$

The first term in this expression corresponds to the distortion energy of the solute (i.e., the energy spent to polarize the chromophore); the second term is the solute−solvent interaction energy that in turn can be split in the electrostatic and van der Waals contributions.

COMPUTATIONAL DETAILS

Geometry optimization was performed with the complete active self-consistent field (CASSCF)[53] theory both in gas phase and in solution. On the basis of our previous experience with the *p*-coumaric acid,[32] the selected basis set was cc-pVDZ and the active space was the complete valence π space with 14 electrons in 12 orbitals (14,12). Ground state minima where calculated as a state averaged of the first five states (SA(5)) with equal weights. For the sake of comparison and completeness, we also ran some tests with DFT-B3LYP and tried a more complete active space (16,13) where the carboxylic oxygen lone pair was included. In order to evaluate the error of using a medium size basis set, we also ran some calculations with aug-cc-pVDZ and cc-pVTZ basis sets.

During the ASEP/MD procedure, the solute charge distribution was described using potential fitted charges calculated at CASSCF(14,12)/cc-pVDZ level. Charges were placed only on nuclei. Consequently, the charges on the heteroatoms could be overestimated as their value must make up for the electrostatic field produced by the lone pairs.[54]

Whereas CASSCF takes into account the near-degeneracies of different electronic configurations, the dynamic correlation energy is not included. Previous studies have evidenced the importance that the consideration of the dynamic correlation has for an adequate description of the absorption spectra of organic molecules.[32,55] This component was considered in the calculation of the vertical transition energies by using CASPT2 methodology.[56,57] In these calculations, the SA(5)-CASSCF wave functions were used as reference.

In solution calculations were performed with the ASEP/MD[36] using Gromacs[58,59] and Molcas-7.6[60] for the molecular dynamics and quantum calculations, respectively. Because of the limited size of the basis set and in order to facilitate comparison with the experiment, we used a value of 0.0 for the ionization potential−electron affinity (IPEA) shift in the CASPT2 calculation. To minimize the appearance of intruder states, an additional imaginary shift of 0.1i E_h was used. The oscillator strengths were calculated with the RASSI algorithm implemented in Molcas.

The molecular dynamics simulations included 1532 water molecules and one molecule of solute in a rhombic dodecahedral box. All molecules had fixed intramolecular geometry. For the solute, the Lennard-Jones parameters were taken from the optimized potentials for liquid simulations, all atoms (OPLS-AA) force field,[61] and the atomic charges were obtained from the quantum calculations. For water molecules, the TIP4P[62] model was employed. Periodic boundary conditions were applied in all directions. Short-range electrostatic interactions were cutoff at 1.3 nm, and long-range interactions were calculated with the particle-mesh Ewald (PME) method.[63] The temperature was fixed at 298 K with the Nosé−Hoover thermostat.[64] Each simulation was run in the NVT ensemble for 500 ps, with a time step of 1 fs, where the first 200 ps were used for equilibration and the last 300 ps for production. In solution, final results were obtained by averaging the last five ASEP/MD cycles, and therefore, they represent a 1.5 ns average.

RESULTS

Electronic and structural properties for different models of the PYP chromophore were compared as a function of the chemical nature of the coumaryl tail. We studied the acid (pCA^-), thio acid ($pCTA^-$), methyl ester ($pCMe^-$), and thiomethyl ester ($pCTMe^-$) derivatives of the anionic *p*-coumaric acid (see Figure 1). Gas phase and in-solution results were compared to elucidate the solvent effects on the vertical absorption of each of the four derivatives. We will start our discussion by analyzing gas-phase results. It is known that the excited states of the chromophore anionic forms are metastable in the gas phase. They become stable states in polar solvents or in whatever

DOI: 10.1021/acs.jpca.5b01434
J. Phys. Chem. A 2015, 119, 5504−5514

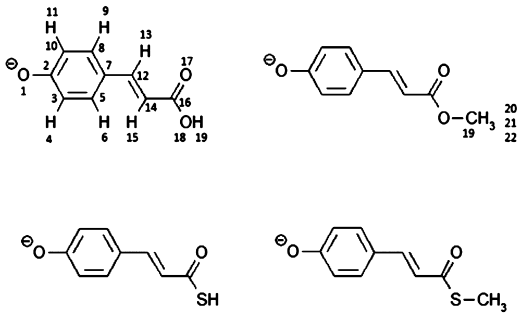

Figure 1. Acid (pCA^-), thioacid ($pCTA^-$), methyl ester ($pCMe^-$), and methyl thioester ($pCTMe^-$) derivatives of the anionic *p*-coumaric acid studied in this paper.

other medium where their negative charge could be stabilized mainly through a network of hydrogen bonds. The mechanism behind this stabilization can be analyzed by comparing the behavior of the system in different environments.

Gas Phase. We started by testing the influence of the active space, calculation level, and basis set on the geometry and vertical transitions of $pCMe^-$ and $pCTMe^-$.

DFT-B3LYP, CASSCF(14,12), and CASSCF(16,13) results were compared by using the cc-pVDZ basis set. The (14,12) active space includes the complete π space and the lone pair from the phenolic oxygen. The potential effect of the electronic states related with the carboxylic oxygen lone pair is puzzled out with the larger active space, (16,13). Table S1 of the Supporting Information collects some selected geometrical parameters. The active space has a small influence on the geometry as CASSCF(14,12) and CASSCF(16,13) give practically the same results. In turn, our DFT values are consistent with previous studies providing double and single bonds longer and shorter, respectively, than CASSCF calculations. The molecule displays a quinonic character, previously reported in literature, especially in the ring. These conclusions are equally valid for methyl ester and methyl thioester derivatives.

Vertical transition energies are shown in Table 1 along with the available experimental data. The values are CASPT2

Table 1. Gas Phase CASPT2 Vertical Transition Energies (eV) for $pCMe^-$ and $pCTMe^-$ at Different Levels of Calculation

	ΔE^0 (S0 → S1)		ΔE^0 (S0 → S2)	
	$pCMe^-$	$pCMeT^-$	$pCMe^-$	$pCMeT^-$
SA-CASSCF(14,12)-PT2//CASSCF(14,12)	2.94	2.73	3.65	3.47
SA-CASSCF(16,13)-PT2//CASSCF(16,13)	2.91	2.69	3.61	3.42
SA-CASSCF(14,12)-PT2//B3LYP	2.86	2.66	3.54	3.36
SA-CASSCF(16,13)-PT2//B3LYP	2.83	2.63	3.49	3.32
Exp.	2.88[a]	2.70 (pCT^-)[b]	–	–

[a]T. Rocha-Rinza et al.[22] [b]Nielsen et al.[19]

energies calculated by using CASSCF wave functions as reference. SA-CASSCF(14,12)-PT2//B3LYP and SA-CASSCF-(16,14)-PT2//B3LYP denote calculations with DFT-optimized geometry.

In all cases, the bright state corresponds to the first excited state, with oscillator strength close to one. This is a $\pi-\pi^*$ transition involving the orbitals displayed in Figure 2. The second excited state is the $n-\pi^*$ state involving the phenolic

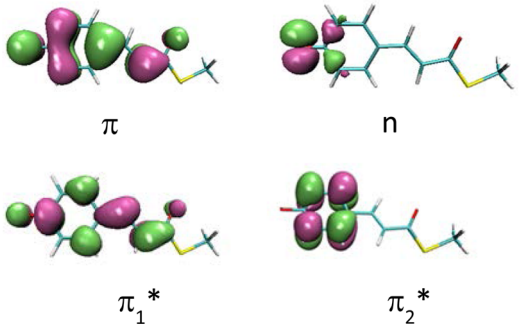

Figure 2. Gas phase and in solution molecular orbitals involved in the main electronic transitions.

oxygen lone pair, and the third one corresponds to a $\pi-\pi^*$ transition where the antibonding orbital is displayed in Figure 2. CASSCF(16,13)-PT2//CASSCF(16,13) and CASSCF-(14,12)-PT2//CASSCF(14,12) transition energies differ in less than 0.05 eV for any state, proving the small influence that the inclusion of the carboxylic oxygen lone pair in the active space has in the final geometry. Actually, this difference can be attributed to the effect of the active space on the energy calculation as (14,12) and (16,13) values using the same B3LYP geometry lead to similar transition energy differences. In any case, the influence of the active space is practically negligible, and results with (14,12) or (16,13) are mostly equivalent. B3LYP geometry yields to transition energies slightly lower (≈ 0.07 eV) than CASSCF ones.

As the larger active space (16,13) includes the carboxylic oxygen lone pair, it permits the study of the $n \rightarrow \pi^*$ transition involving this orbital. This state appears as the fifth excited state for the methyl thioester derivative (4.35 eV) and as the eighth for the methyl ester one (5.33 eV). Being so high in energy, it does not interfere in the position of the absorption band. In fact, there is almost no difference between (14,12) and (16,13) results. Consequently, we use the less computional-demanding (14,12) active space in the rest of this paper.

A quite good agreement is found between the calculated transition energies and the available experimental data. Thus, the absorption maximum for the methyl ester derivative is experimentally found at 2.88 eV,[22] whereas CASSCF(14,12)-PT2//CASSCF(14,12) and CASSCF(14,12)-PT2//B3LYP values are 2.94 and 2.86 eV, respectively. Although there is no experimental data for the methyl thioester, the absorption spectrum for the phenyl thioester (pCT^-) derivative has been registered and the maximum is found at 2.70 eV.[19] This value is a good reference for $pCTMe^-$ as the electron conjugation does not extend beyond the sulfur atom. It can be noted a good agreement between this experimental result and the calculated values (2.73 and 2.66 eV for CASSCF(14,12)-PT2//CASSCF-(14,12) and CASSCF(14,12)-PT2//B3LYP).

We have also run some tests in order to evaluate the error due to using a medium size basis set as cc-pVDZ. To this end, transition energies were recalculated with B3LYP/cc-pVTZ and B3LYP/aug-cc-pVDZ optimized geometries. These CASSCF-(14,12)-PT2//B3LYP results are collected in Table 2. As it has been previously reported,[26] the introduction of diffuse functions decreases the transition energies. The triple-ζ basis set (cc-pVTZ) follows the same trend. In general, the influence

DOI: 10.1021/acs.jpca.5b01434
J. Phys. Chem. A 2015, 119, 5504−5514

Table 2. Gas Phase SA-CASSCF(14,12)-PT2//B3LYP Transition Energies (eV) Calculated with Different Basis Sets

	ΔE^0 (S0 → S1)		ΔE^0 (S0 → S2)	
	pCMe$^-$	pCMeT$^-$	pCMe$^-$	pCMeT$^-$
cc-pVDZ	2.86	2.66	3.54	3.36
aug-cc-pVDZ	2.64	2.34	3.49	3.28
cc-pVTZ	2.73	2.52	3.52	3.34

of the basis set on the transition energies of these systems is small. It is worth noting the slight deviation of the CASPT2 results from the experiment when more complete basis sets are used. This fact can be related with the use of a 0.0 value for the IPEA. An IPEA value of 0.25 has been proposed when larger basis sets are used.[60] Therefore, attending to a performance criterion, we used the simplest cc-pVDZ for the rest of our calculations.

In sum, in gas phase the active space and the employed quantum method for geometry optimization have only a small effect on the transition energies. Good agreement with the available experimental data is reached in all cases. In an upcoming paper, we will tackle the different deactivation path for the excited state of the PYP chromophore as a function of the terminal group. Given that the use of TD-DFT in the study of charge transfer states and in the neighborhood of conical intersections has been criticized[65,66] and in order to have a set of comparable results both in the ground and in the excited potential surfaces, we decided to continue our study at the CASSCF(14,12)/cc-pVDZ level of calculation, as multireference methods have demonstrated their suitability in this field.

Table 3 presents transition energies and dipole moments of pCA$^-$, pCMe$^-$, pCTA$^-$, and pCTMe$^-$. In charged systems, the dipole moment value depends on the position of the origin of coordinates, consequently, only relative variations referred to the same origin, as it is the case, are meaningful. Regarding the electronic spectra, the bright excited state for the four derivatives appears as the first excited state with a value for the oscillator strength close to the unit. The implied orbitals are equivalent to those shown in Figure 2. Transition energies are all in the same order of magnitude even if they can be classified into two groups: on the one hand pCA$^-$ and pCMe$^-$ and on the other hand pCTA$^-$ and pCTMe$^-$. The presence of sulfur in the structure results in a slight red shift of the first absorption band of around 0.21 eV, which agrees very well with the experimental red shift (0.18 eV). On the contrary, the substitution of the terminal hydrogen for the methyl group does not modify the band position. Even though, to our knowledge, no experimental values have been published for pCTA$^-$ and pCTMe$^-$ in the gas phase, several derivatives of the anionic *trans-p*-coumaric acid have been theoretically studied. The vertical excitation energy of pCA$^-$ has been profusely studied with a vast variety of theoretical methods.[22,24,26,29] Our results are in line with the value (2.98 eV) published by Zuev et al.[24] using a similar level of calculation (SS-CASPT2/ANO-RCC-VTZP). For the methylate compounds, Gromov et al.[26] reported CC2/cc-pVDZ and EOM-CCSD/cc-pVDZ transition energies of 3.27 and 3.35 eV for pCMe$^-$ and 3.10 and 3.17 eV for pCTMe$^-$. Even though these results slightly overestimate the experimental energy, they show a red-shifting effect of the sulfur atom on the absorption band. At the CC2/SV(P) level of calculation, these authors[28] reported a more accurate value of 2.89 eV for the absorption of pCTMe$^-$. It is important to note that all TD-DFT published results for the anion overestimate experimental excitation energies. So, Muguruza et al.[65] reported values of 3.40 and 3.28 eV for the vertical energies of pCTMe$^-$ and pCT$^-$ derivatives at PBE TD-DFT level of calculation and Sergi et al.,[66] a value of 3.24 eV for pCA$^-$. In accordance with these values, it seems evident the poor performance of this method in describing charge-transfer excited states. As for the thioacid derivative, as far as we know, there are no previous theoretical or experimental studies on the vertical absorption energies.

Table 3. SA-CASSCF(14,12)-PT2/cc-pVDZ Dipole Moment Values (D) and Transition Energies (eV) in Gas Phase

	pCA$^-$	pCMe$^-$	pCTA$^-$	pCTMe$^-$
		Dipole		
S0	7.82	8.03	4.70	5.29
S1($\pi \rightarrow \pi_1^*$)	4.66	4.61	3.33	3.39
S2(n $\rightarrow \pi_1^*$)	1.65	1.76	4.06	3.66
S3($\pi \rightarrow \pi_2^*$)	11.41	11.53	8.86	9.39
		Transitions (ΔE^0)		
Exp.	2.89[a]	2.88[a]	–	2.70 (pCT$^-$)[b]
S0−S1($\pi \rightarrow \pi_1^*$)	2.96	2.94	2.73	2.73
S0−S2(n $\rightarrow \pi_1^*$)	3.65	3.65	3.45	3.47
S0−S3($\pi \rightarrow \pi_2^*$)	3.82	3.81	3.88	3.86

[a]T. Rocha-Rinza et al.[22] [b]Nielsen et al.[19]

Table 4 collects the atomic point charges for the different compounds in the ground and excited states. In order to simplify the analysis, the molecule has been divided in three parts (phenolic ring, central double bond, and the acid or ester terminal group). It is well-established, see for instance Gromov et al.,[26] that the ground state of the PYP features a large negative charge on the phenolic group and that during the electronic transition part of this charge is transferred toward the rest of the molecule. Our aim in this regard is to compare this behavior when the substituent is modified. All the compounds follow the same trend, although with some small differences. Thus, one can observe that the ground state of pCA$^-$ and pCMe$^-$ present a greater negative charge on the phenolic and central part of the molecule than pCTA$^-$ and pCTMe$^-$ which, due to the better electron-acceptor character of the sulfur, present a larger charge over the thioester group and consequently lower dipole moment values. As for the flux of charge during the electronic transition, it is larger for pCA$^-$ and

Table 4. Gas Phase Potential Fitted Charges at CASSCF(14,12)/cc-pVDZ level

	pCA$^-$		pCMe$^-$		pCTA$^-$		pCTMe$^-$	
	GS	$\pi \rightarrow \pi_1^*$	GS	$\pi \rightarrow \pi_1^*$	GS	$\pi \rightarrow \pi_1^*$	GS	$\pi \rightarrow \pi_1^*$
ring	−0.615	−0.398	−0.626	−0.398	−0.589	−0.462	−0.595	−0.446
double bond	−0.308	−0.433	−0.358	−0.487	−0.209	−0.232	−0.287	−0.323
coumaryl end	−0.077	−0.169	−0.016	−0.115	−0.202	−0.307	−0.118	−0.231

DOI: 10.1021/acs.jpca.5b01434
J. Phys. Chem. A 2015, 119, 5504−5514

pCMe$^-$, ≈ 0.22 e, than in pCTA$^-$ and pCTMe$^-$, ≈ 0.13 e. Furthermore, whereas in the oxy derivate the increase in negative charge is almost equally shared by the double bond and the terminal group (COOH or $COOCH_3$) in pCTA$^-$ and pCTMe$^-$, the charge mainly accumulates in the thio end. This fact evidences the larger electronic affinity of the sulfur atom versus the oxygen. In any case, the displacement of the negative charge from the phenolic oxygen toward the rest of the molecule fits with the observed decrease of the dipole moment in the excited state. As we see, transition energies, dipole moments, and charge distribution variations are all consistent, and all of them yield the same conclusions.

Water Solution. Let us now analyze the effect that the interaction with water introduces on the structural and electronic properties of our four models for the PYP chromophore. As it was said before, the in solution study was performed with the ASEP/MD method.[31]

With regard to the geometry, there are no significant differences between the ground state minima for any of the four compounds in water solution (See Table S2 of the Supporting Information). Only the bond lengths involving the oxygen or sulfur final atoms show different behavior. Nevertheless, these geometries are notably different from those obtained in the gas phase, even though they remain essentially planar. There is an important increase of the phenolic oxygen bond length as a result of the interaction with the solvent (1.23 Å in gas phase and 1.28 Å in solution). In addition, a certain loss of the quinonic character displayed in the gas phase can be observed. So, in solution, single bonds are longer and double bonds shorter than in the gas phase. Contrary to what could be expected, the carboxylic double bond length is not modified by the solvent, probably due to the small interaction energy of this group with the solvent. Steric hindrance and the low charge on the carbonyl group (C16O17) are responsible for this fact. The effect of the hydrogen bonds on the properties of the thioester derivative has been studied by Gromov et al. by introducing two water molecules interacting with the phenolate moiety.[26] The bond length variations reported by these authors are clearly smaller than the results presented in our study. This becomes more evident as one passes from the phenolic moiety to the rest of the molecule. In fact, microsolvation induces variations in the bonds of the central part that represent just one-third of those obtained with ASEP/MD. It can be concluded that the presence of only the two water molecules does not adequately represent the complete interaction with the bulk solvent.

In water solution, the spectrum is notably more complex than in the gas phase. Data in Table 5 permit the analysis of the nature of the first three transitions. First it can be noted that, due to its low dipole moment, the n → π^* state is destabilized in solution with respect to the $\pi \rightarrow \pi_2^*$ excited state and it becomes the third excited state. Now, the first two excited states are $\pi \rightarrow \pi^*$ and both display contributions from $\pi \rightarrow \pi_1^*$ and $\pi \rightarrow \pi_2^*$ transitions. Molecular orbitals involved in these transitions are similar to those shown in Figure 2. Oscillator strengths agree with the mixture shown by S1 and S2. In pCA$^-$ and pCMe$^-$, the S1 and S2 states are practically degenerate, even though the brighter state, according to the oscillator strength, is S2. On the contrary, for pCTA$^-$ and pCTMe$^-$, there exist a gap of around 0.35 eV between the first two excited states, S1 remaining the bright one. The mixture between S1 and S2 in solution can be understood taking a look at the large dipole moment of the $\pi \rightarrow \pi_2^*$ excited state in the gas phase. This state is more stabilized by the solvent than $\pi \rightarrow \pi_1^*$ and n → π_1^*, becoming the first excited state for pCA$^-$ and pCMe$^-$. In fact, the $\pi \rightarrow \pi_2^*$ state is the only one for which a slight red shift ($\delta \approx -0.05$ eV) is found in solution. So, it can be concluded that in solution the thio compounds show S1 and S2 excited states moderately well-separated, whereas these states are completely degenerate for the oxy derivatives. As said before, this fact is related to the larger dipole moment shown by the $\pi \rightarrow \pi_2^*$ state for the oxy compound as a consequence of a more localized negative charge in the phenyl moiety. The differences in the relative stabilities of $\pi \rightarrow \pi^*$ states of oxy and thio derivatives could be related with the different de-excitation routes that pCT$^-$ and pCMe$^-$ follow in polar solvents. Whether the degeneracy of S1 and S2 makes the isomerization path accessible for the oxy derivatives is a fact that will be addressed in a future paper.

In any case, and following the trend observed in the gas phase, transition energies for those bright states of pCA$^-$ and pCMe$^-$ (≈3.8 eV) are slightly larger than those corresponding to the thio analogues (≈3.5 eV). This difference (≈ 0.3 eV) is practically the same than that found in the gas phase (≈0.2 eV). In solution, the absorption bands are shifted toward shorter wavelengths. This blue shift is related to the stabilization of localized charges by polar solvents. In fact, all the four derivatives have, in their ground states, a larger negative charge in the phenyl group when in solution than in gas phase (Tables 4 and 6). In solution, the negative charge hosted by the central double bond is completely shifted toward the phenolic moiety.

Table 5. In Solution SA-CASSCF(14,12)-PT2/cc-pVDZ Dipole Moment Values (D), Transition Energies (eV), Oscillator Strengths, and Solvent Shifts (eV)[a]

	pCA$^-$	pCMe$^-$	pCTA$^-$	pCTMe$^-$
		Dipole		
S0	16.24	18.85	17.61	19.89
S1	14.80	17.80	11.34	14.08
S2	9.54	12.02	15.12	17.08
S3(n → π_1^*)	5.76	8.51	6.39	8.78
		Transitions (ΔE)		
Experimental	–	3.48−3.54[b]	–	3.22−3.26[c]
S0−S1	3.76	3.76	3.46	3.48
($\pi \rightarrow \pi_1^*$)	20%	18%	51%	49%
($\pi \rightarrow \pi_2^*$)	37%	39%	14%	16%
S0−S2	3.78	3.81	3.84	3.82
($\pi \rightarrow \pi_1^*$)	48%	49%	18%	20%
($\pi \rightarrow \pi_2^*$)	13%	13%	37%	36%
S0−S3	4.97	5.0	4.86	4.86
(n → π_1^*)	72%	76%	76%	76%
		Oscillator Strength (f)		
S0−S1	0.2	0.18	0.51	0.49
S0−S2	0.6	0.60	0.28	0.31
S0−S3	≈0	≈0	≈0	≈0
		Solvent Shift (δ)		
S0−S1	−0.06	−0.05	0.73	0.75
S0−S2	0.82	0.87	−0.04	−0.04
S0−S3	1.32	1.35	1.41	1.39

[a]With regard to the experimental data of pCA$^-$ and pCTA$^-$ in solution, as the basicity increases the monoanion species present in the medium would be the carboxylate anion due to the bigger acidity of this hydrogen atom. Consequently, no experimental data are available for the phenolate anions pCA$^-$ and pCTA$^-$. [b]Rocha-Rinza el al.[22] [c]Nassem et al.[68] and Larsen et al.[69]

DOI: 10.1021/acs.jpca.5b01434
J. Phys. Chem. A 2015, 119, 5504−5514

Table 6. In Solution Potential Fitted Charges at CASSCF(14,12)/cc-pVDZ Level

	pCA$^-$		pCMe$^-$		pCTA$^-$		pCTMe$^-$	
	GS	$\pi \rightarrow \pi_1^*$	GS	$\pi \rightarrow \pi_1^*$	GS	$\pi \rightarrow \pi_1^*$	GS	$\pi \rightarrow \pi_1^*$
ring	−0.855	−0.510	−0.844	−0.511	−0.956	−0.627	−0.917	−0.619
double bond	−0.156	−0.418	−0.278	−0.526	0.072	−0.172	−0.134	−0.360
coumaryl end	0.012	−0.071	0.122	0.036	−0.116	−0.201	0.050	−0.021

When the vertical transition in solution takes place, as a nonequilibrium solvent is considered according to the Franck−Condon principle, the solvent penalizes the charge transference from the phenolic part toward the rest of the molecule. Consequently, a blue shift is expected.

The calculated solvent shifts of the bright states are about 0.73−0.87 eV. These values overestimate in 0.21 eV the experimental one. In turn, this fact is related to the overestimation of the transition energies in solution. One of the possible origins for this is the use of CASSCF optimized geometries. It is known that the CASSCF method overestimates the charge separation, and consequently, it leads to an overestimation of the solute−solvent interaction energies.

Table 6 permits the analysis of the charge distribution and the fluxes of charge during the excitation to the bright state. The four derivatives show a flux of charge from the phenolic part to the other two moieties. It is interesting to note that the negative charge transferred is practically the same in all cases: about 0.32 e from the phenolic part to the central double bond (0.24 e) and the terminal moieties (0.08 e). That leads to a more smoothed out negative charge along the molecule as it happened in the gas phase. Consequently, dipole moments decrease in about 30−35% during the transition. In any case, it is remarkable the correlation between the localization of the negative charge in the phenyl moiety and the increase in the dipole moment value.

Figures 3 and 4 display the H(water)−O1(solute), H(water)−O17(solute) pair radial distribution functions (rdfs)

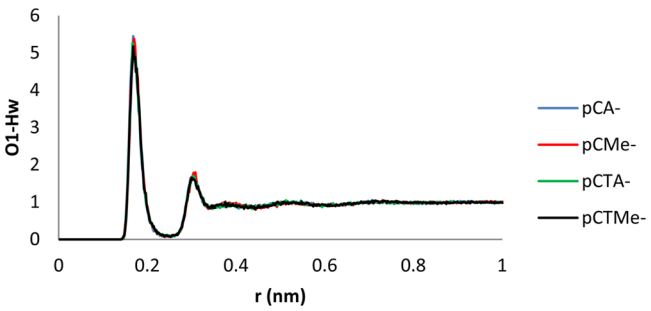

Figure 3. Radial distribution function corresponding to the pair O1(solute)−H(water).

for the four studied derivatives and Figure 5 the corresponding rdfs between the H(water) and S18 for the thio-derivatives or O18 for pCA$^-$ and pCMe$^-$. Whereas the height of the first peak is equivalent in the H−O1 rdfs for all the derivatives, this is not the case for H−O17. The solvent is less structured around the carboxylic oxygen of thio-derivatives. Coordination numbers in Table 7 are in agreement with this fact, even though differences are quite subtle. The differences between the solvent structure around O1 and O17 are remarkable. As for atom 18 (O for pCA$^-$ and pCMe$^-$ or S for pCTA$^-$ and pCTMe$^-$), the solvent does not present a relevant structure, although it is somewhat more visible for pCA$^-$ and pCMe$^-$.

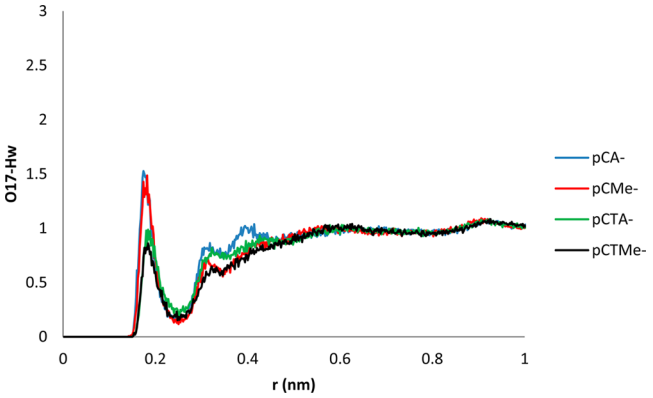

Figure 4. Radial distribution function corresponding to the pair O17(solute)−H(water).

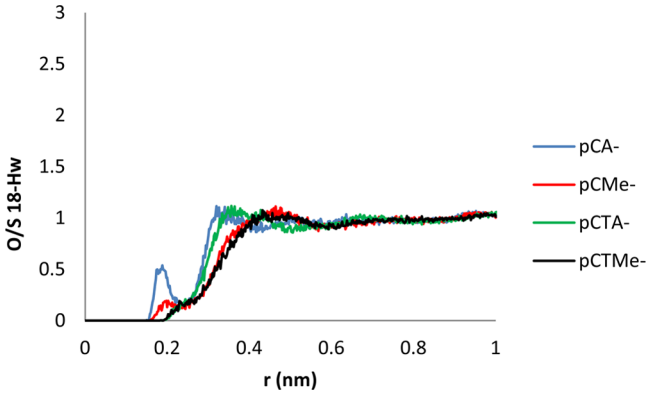

Figure 5. Radial distribution function corresponding to the pair S18(solute)−(water) for pCTA$^-$ and pCTMe$^-$ and to the pair O18(solute)−H(water) for pCA$^-$ and pCMe$^-$.

Table 7. Coordination Numbers

	H-O1	H-O17	H-O18/H-S18
pCA$^-$	2.1	0.9	0.4
pCMe$^-$	2.1	0.9	0.2
pCAT$^-$	2.1	0.7	0.1
pCTMe$^-$	2.1	0.6	0.1

A quantity that can be useful in the analysis of the results is the group contribution to the solute−solvent interaction energy (Table 8). The molecules have been divided in four parts: the phenolic oxygen, the phenyl group, the central double bond, and the terminal part (acid, thioacid, ester, or thioester, depending on the case). The larger contribution to the total interaction energy comes from the phenolic oxygen. However, the contributions of the remaining groups are far from being negligible. Interaction energies correlate with the charges sustained by the different groups (see Table 6). Thus, the general trend is an increase of the solute−solvent interaction energy with the charge. Nevertheless, there are exceptions, and

DOI: 10.1021/acs.jpca.5b01434
J. Phys. Chem. A 2015, 119, 5504−5514

Table 8. Solute−Solvent Interaction Energies (kcal/mol)

	GS					$\pi \rightarrow \pi_1^*$				
	O	Ph	C=C	COXY	Total	O	Ph	C=C	COXY	Total
pCA^-	−158.45	16.85	−6.41	−24.61	−172.91	−139.82	34.51	−17.62	−27.62	−150.54
$pCMe^-$	−149.10	14.18	−10.75	−10.27	−155.93	−131.81	31.47	−21.85	−13.35	−135.54
$pCTA^-$	−147.57	9.41	2.21	−15.38	−151.33	−129.04	24.59	−7.35	−18.17	−129.97
$pCTMe^-$	−148.56	12.52	−4.22	−5.64	−145.90	−131.42	25.77	−13.53	−8.15	−127.34
	GS				$\pi \rightarrow \pi_1^*$			
	CO	X	Y	Total (COXY)	CO	X	Y	Total (COXY)
pCA^-	−4.85	−14.84	−4.92	−24.61	−7.57	−15.07	−4.98	−27.62
$pCMe^-$	−1.07	−10.68	1.48	−10.27	−3.96	−10.88	1.48	−13.35
$pCTA^-$	−6.92	−5.62	−2.84	−15.38	−9.50	−5.81	−2.86	−18.17
$pCTMe^-$	1.28	−7.26	0.34	−5.64	−0.97	−7.42	0.24	−8.15

it is remarkable the large contribution of the terminal part even though its total charge is very small. In order to understand this behavior, we split the contribution of the terminal part in three contributions: carbonyl, oxygen, or sulfur atom and hydrogen or the methyl group. Even though the total charge of the COXY (X = O or S, Y = H or CH_3) terminal part is small, it is not the case for each of its members. So, the interaction energy from the terminal oxygen and sulfur atoms is the most important contribution to the total interaction energy of the COXY group, being oxygen contribution bigger than the corresponding sulfur contribution. It is also interesting to note that the H or CH_3 contributions to the solute−solvent interaction energy are attractive and repulsive, respectively. Nevertheless, these contributions are minor and are not responsible for the differences between derivatives. These results are in line with the small influence that the methyl or hydrogen atoms have in other molecular properties.

Electronic transition results in a decrease of the solute−solvent interaction energy. This is mainly due to the decrease of ca. 35−40 kcal in the contribution of the phenolic part of the molecule (Ph−O). This fact is related to a charge shift of around 35% from this moiety to the rest of the molecule during the transition and with the solvent structure around the solute molecule in equilibrium with the ground state. O17 presents a reduced number of water molecules placed in its neighborhood compared to the number around the phenolic oxygen, and consequently, the transferred charge is not so effectively stabilized by the solvent. A similar conclusion was obtained in a previous paper[67] where the solvent structure around the $pCMe^-$ was analyzed both in the ground and excited state.

Finally, it is remarkable that the contribution of the terminal group to the total solute−solvent interaction energy is almost invariable. This fact evidences again the minimal participation of this part of the molecule during the electronic transition.

That the most important interaction with the solvent is centered in the phenolic oxygen is the reason why the microsolvation on this part of the molecule is used with the aim of roughly mimicking the effect of the condensed medium. So, Gromov et al.[26] calculated a value of 2.96 eV for the $pCTMe^-$ with two water molecules placed close to the phenolic oxygen (CC2/aug-cc-pVDZ). This value is in reasonable agreement with the experimental value of 3.22 eV published by Naseem et al.[68] Nevertheless, those authors arrive to a theoretical solvent shift of 0.05 eV as they found the absorption band in the gas phase at 2.91 eV. This value is clearly underestimated when compared to the experiment. Assuming the gas phase experimental value for pCT^- (2.70 eV) as suitable reference value for $pCTMe^-$ too, the experimental solvent shift can be estimated in 0.52 eV. Therefore, in this case, the microsolvation does not account for the total effect of the solvent as microsolvated and gas phase results are practically equivalent.

Wang et al.[33] studied $pCTMe^-$ in various solvents with different dielectric constants using CPCM/TD-B3LYP. In water, the absorption energy was calculated to be 3.03 eV, lower than the value obtained in the gas phase (3.17 eV). Consequently, a red shift contrary to the experimental result was obtained. Probably, this poor performance is related with the neglect of specific solute−solvent interactions by CPCM, although the suitability of TD-B3LYP in the description of the charge fluxes during the electronic transitions in $pCTMe^-$ could also be questioned. In any case, ASEP/MD, where solvent−solute specific interactions are taken into account, yields values of 3.47 and 0.73 eV for the in-solution vertical absorption and solvent shift, respectively, in good agreement with the experiment, even though the solvent shift is slightly overestimated. So, we must conclude that the representation of the solvent through a few solvent molecules or making use of continuum methods does not accurately account for the solvation effects on the studied systems. In the first case because solvation is a global property hardly represented just through a few solvent molecules and in the second because specific interaction between solute and solvent are missing.

CONCLUSIONS

In this paper, we have addressed the possible influence of the terminal group and solvent on the absorption spectrum of several *p*-coumaric derivatives. Sulfur versus oxygen and hydrogen versus methyl substituents have been analyzed. We find that the replacement of the H19 hydrogen atom by a methyl group has no effect on the transition energies, even though a clear loss of the solvent structure can be observed when the hydrogen terminal atoms is replaced by the methyl group. This fact evidences the slight participation of this part of the molecule in the flux of charge that characterizes the electronic transition.

With regard to the electronic spectra of the studied derivatives, their transition energies can be put into two groups: on the one hand, pCA^- and $pCMe^-$, and on the other hand, $pCTA^-$ and $pCTMe^-$. In gas phase, the bright state is the first excited state with a $\pi \rightarrow \pi_1^*$ character. This state is followed in energy by the states corresponding to the $n \rightarrow \pi_1^*$ and $\pi \rightarrow \pi_2^*$ transitions. With regard to S1 ($\pi \rightarrow \pi_1^*$), slightly red-shifted absorption bands (≈0.20 eV) were calculated for $pCTA^-$ and $pCTMe^-$ with respect to pCA^- and $pCMe^-$. For

DOI: 10.1021/acs.jpca.5b01434
J. Phys. Chem. A 2015, 119, 5504−5514

all of them, this state shows a similar and strong charge transfer character. For S2 (n → π_1*) and S3 ($\pi \rightarrow \pi_2$*), the presence of sulfur produces a red (≈0.20 eV) and blue (≈0.05 eV) shift, respectively.

In solution, the spectrum changes substantially with respect to that obtained in the gas phase. The n → π_1* state is destabilized by a polar solvent like water, and it becomes the third excited state in solution suffering an important blue shift. Now, $\pi \rightarrow \pi_1$* and $\pi \rightarrow \pi_2$* states mix, and contributions of both transitions are found in S1 and S2. The presence of the sulfur modulates the solvent effect, and the first two excited states become practically degenerate for pCA^- and $pCMe^-$ but moderately well-separated for $pCTA^-$ and $pCTMe^-$. As for the solvent shift, the bright state experiences a blue shift in water solution of 0.73−0.87 eV. This value overestimates the experimental data mainly due to the overestimation of the charge separation provided by CASSCF. Although in this system there are several polar groups present, the solvent shift seems to be mainly determined by the solvation of the phenolic oxygen. Finally, it is remarkable the small influence of the solvation on the $\pi \rightarrow \pi_2$* transition. The nature of this transition, totally restricted to the phenyl ring, is responsible for this behavior.

In sum, we have found some differences in the absorption spectra of oxy and thio derivatives that could shed light on the different behavior exhibited by pCT^- and $pCMe^-$ in solution. The mixture between $\pi \rightarrow \pi_1$* and $\pi \rightarrow \pi_2$* in water solution for S1 and S2 and the fact that for the oxy derivatives the bright state is S2 could be the cause for the different relaxation dynamics and pathways during the de-excitation. Different routes can be activated to permit the photoisomerization of $pCMe^-$ in methanol but not for pCT^- in water after irradiation at 440 nm. Further studies on the de-excitation path for these derivatives are required in order to elucidate the differences during the photoisomerization process in solution. Finally, we have shown that neither microsolvation with a few solvent molecules nor continuum models correctly account for the total effect of the solvent for PYP derivatives. We must conclude that solvation is a global property that is hardly represented without taking into account specific interactions in a large enough solvent volume.

■ ASSOCIATED CONTENT

Supporting Information

Gas phase DFT, CASSCF(14,12), and CASSCF(16,13) intramolecular parameters for $pCMe^-$ and $pCTMe^-$ using the cc-pVDZ basis. Gas phase and in-water solution intermolecular parameters for the ground state of pCA^-, $pCMe^-$, $pCTA^-$, and $pCTMe^-$ optimized at the CASSCF(14,12)/cc-pVDZ level. The Supporting Information is available free of charge on the ACS Publications website at DOI: 10.1021/acs.jpca.5b01434.

■ AUTHOR INFORMATION

Corresponding Authors

*E-mail: maguilar@unex.es.
*E-mail: memartin@unex.es.

Notes

The authors declare no competing financial interest.

■ ACKNOWLEDGMENTS

This work was supported by the GR10048 Project from the Consejería de Economía, Comercio e Innovación of the Gobierno de Extremadura. F.F.G-P. acknowledges a fellowship from the Ministerio de Educación y Ciencia.

■ REFERENCES

(1) Kukura, P.; McCamant, D. W.; Yoon, S.; Wandschneider, D. B.; Mathies, R. A. Structural Observation of the primary isomerization in vision with femtosecond-stimulated Raman. *Science* **2005**, *310*, 1006−1009.

(2) Braiman, M.; Mathies, R. A. Resonance Raman spectra of bacteriorhodopsin's primary photoproduct: Evidence for a distorted 13-cis retinal chromophore. *Proc. Natl. Acad. Sci. U.S.A.* **1982**, *79*, 403−407.

(3) Larsen, D. S.; van Grondelle, R. Initial photoinduced dynamics of the photoactive yellow protein. *ChemPhysChem* **2005**, *6*, 828−837.

(4) Meyer, T. E. Isolation and characterization of solute cytochromes, ferredoxins and other chromophoric protein from the halophilic phototrophic bacterium Ectothiorhodospira halophila. *Biochim. Biophys. Acta* **1985**, *806*, 175−183.

(5) Meyer, T. E.; Yakali, E-; Cusanovich, M. A.; Tollin, G. Properties of a water-soluble, yellow protein isolated from a halophilic phototrophic bacterium that has photochemical activity analogous to sensory rhodopsin. *Biochemistry* **1987**, *26*, 418−423.

(6) Hellingwerf, K. J.; Hendriks, J.; Gensch, T. Will this "Yellow Lab" bring us where we want to go? *J. Phys. Chem. A* **2003**, *107*, 1082−1094.

(7) Hoff, W. D.; Dux, P.; Hard, K.; Devreese, B.; Nugteren-Roodzant, I. M.; Crielaard, W.; Boelens, R.; Kaptein, R.; Beeumen, J.; Hellingwerf, K. J. Thiol ester-linked *p*-coumaric acid as a new photoactive prosthetic group in a protein with rhodopsin-like photochemistry. *Biochemistry* **1994**, *33*, 13959−13962.

(8) Kort, R.; Vonk, H.; Xu, X.; Hoff, W. D.; Criellard, W.; Hellingwerf, K. J. Evidence for *trans-cis* isomerization of the *p*-coumaric acid chromophore as the photochemical basis of the photocycle of photoactive yellow protein. *FEBS Lett.* **1996**, *382*, 73−78.

(9) Xie, A.; Hoff, W. D.; Kroon, A. R.; Hellingwerf, K. J. Glu46 donates a proton to the 4-hydroxycinnamate anion chromophore during the photocycle of photoactive yellow protein. *Biochemistry* **1996**, *35*, 14671.

(10) Unno, M.; Kumauchi, M.; Sasaki, J.; Tokunaga, F.; Yamaguchi, S. Evidence for a protonated and cis configuration chromophore in the photobleached intermediate of photoactive yellow protein. *J. Am. Chem. Soc.* **2000**, *122*, 4233−4234.

(11) Genik, U. K.; Soltis, S. M.; Kuhn, P.; Canestrelli, I. L.; Getzoff, E. D. Structure at 0.85 A resolution of an early protein photocycle intermediate. *Nature* **1998**, *392*, 206−209.

(12) Andersen, L. H.; Bochenkova, A. V. The photophysics of isolated protein chromophores. *Eur. Phys. J. D* **2009**, *51*, 5−14.

(13) Rajput, J.; Rahbek, D. B.; Aravind, G.; Andersen, L. H. Spectral tuning of the photoactive yellow protein chromophore by H-bonding. *Biophys. J.* **2010**, *98*, 488−492.

(14) Espagne, A.; Changenet-Barret, P.; Plaza, P.; Martín, M. M. Solvent effect on the excited-state dynamics of analogues of the photoactive yellow protein chromophore. *J. Phys. Chem. A* **2006**, *110*, 3393−3404.

(15) Espagne, A.; Paik, D. H.; Changenet-Barret, P.; Plaza, P.; Martín, M. M.; Zewail, A. H. Ultrafast light-induced response of photoactive yellow protein chromophore analogues. *Photochem. Photobiol. Sci.* **2007**, *6*, 780−787.

(16) Larsen, D. S.; Vengris, M.; Van Stokkum, I. H. M.; van der Hosrst, M. A.; Cordfunke, R. A.; Hellingwerf, K. J.; van Grondelle, R. Initial photo-induced dynamics of the photoactive yellow protein chromophore in solution. *Chem. Phys. Lett.* **2003**, *369*, 563−569.

(17) Vengris, M.; Larsen, S.; van der Horst, M. A.; Larsen, O. F. A.; Hellingwerf, K. J.; van Grondelle, R. Ultrafast dynamics of isolated model photoactive yellow protein chromophores: "Chemical perturbation theory" in the laboratory. *J. Phys. Chem. B* **2005**, *109*, 4197−4208.

DOI: 10.1021/acs.jpca.5b01434
J. Phys. Chem. A 2015, 119, 5504−5514

(18) El-Gezawy, H.; Rettig, W.; Danel, A.; Jonusauskas, G. Probing the photochemical mechanism in photoactive yellow protein. *J. Phys. Chem. B* **2005**, *109*, 18699−18705.
(19) Nielsen, I. G.; Boye-Peronne, S.; El Ghazaly, M. O. A.; Kristensen, M. B.; Nielsen, S. B.; Anderson, L. H. Absorption spectra of photoactive yellow protein chromophores is vacuum. *Biophys. J.* **2005**, *89*, 2597−2604.
(20) Chengenet-Barret, P.; Espagne, A.; Charier, S.; Baudin, J.-B.; Jullien, L.; Plaza, P.; Hellingwerf, K. J.; Martin, M. M. Early molecular events in the photoactive yellow protein: role of the chromophore photophysics. *Photochem. Photobiol. Sci.* **2004**, *3*, 823−829.
(21) Chengenet-Barret, P.; Espagne, A.; Plaza, P.; Hellingwerf, K. J.; Martin, M. M. Investigations of the primary events in a bacterial photoreceptor for photomotility: photoactive yellow protein. *New J. Chem.* **2005**, *29*, 527−534.
(22) Rocha-Rinza, T.; Christiansenm, O.; Rajput, H.; Gopalan, A.; Rahbek, D. B.; Andersen, L. H.; Bochenkova, A. V.; Granovsky, A. A.; Bravaya, K. B.; Nemukhin, A. V.; et al. Gas phase absorption studies of photoactive yellow protein chromophore derivatives. *J. Phys. Chem. A* **2009**, *113*, 9442−9449.
(23) Coto, P. B.; Roca-Sanjuán, D.; Serrano-Andrés, L.; Martín-Pendás, A.; Martí, S.; Andrés, J. Toward understanding the photochemistry of photoactive yellow protein: A CASPT2/CASSCF and quantum theory of atoms in molecules combined study of a model chromophore in vacuo. *J. Chem. Theory Comput.* **2009**, *5*, 3032−3038.
(24) Zuev, D.; Bravaya, K. B.; Crawford, T. D.; Lindh, R.; Krylov, A. I. Electronic structure of the two isomers of the anionic form of p-coumaric acid chromophore. *J. Chem. Phys.* **2011**, *134*, 034310.
(25) Boggio-Pasqua, M.; Robb, M. A.; Groenhof, G. Hydrogen bonding controls excited-state decay of the photoactive yellow protein chromophore. *J. Am. Chem. Soc.* **2009**, *131*, 13580−13581.
(26) Gromov, E. V.; Burghardt, I.; Hynes, J. T.; Köppel, H.; Cederbaum, L. S. Electronic structure of the photoactive yellow protein chromophore: Ab-initio study of the low-lying excited single states. *J. Photochem. Photobiol. A: Chem.* **2007**, *190*, 241−257.
(27) Gromov, E. V.; Burghardt, I.; Köppel, H.; Cederbaum, L. S. Photoinduced isomerization of the photoactive yellow protein (PYP) chromophore: Interplay of two torsions, a HOOP model and hydrogen bonding. *J. Phys. Chem. A* **2011**, *115*, 9237−9248.
(28) Gromov, E. V.; Burghardt, I.; Köppel, H.; Cederbaum, L. S. Electronic structure of the PYP chromophore in its native protein environment. *J. Am. Chem. Soc.* **2007**, *129*, 6798−6806.
(29) Rocha-Rinza, T.; Sneskov, K.; Christiansen, O.; Ryde, U.; Kongsted, J. Unraveling the similarity of the photoabsorption of deprotonated p-coumaric acid in the gas phase and within the photoactive yellow protein. *Phys. Chem. Chem. Phys.* **2011**, *13*, 1585−1589.
(30) Groenhof, G.; Bouxin-Cademartory, M.; Hess, B.; de Visser, S. P.; Berendsen, H. J. C.; Olivucci, M.; Mark, A. E.; Robb, M. A. Photoactivation of the photoactive yellow protein: Why photon absorption triggers a trans-to-cis isomerization of the chromophore in the protein. *J. Am. Chem. Soc.* **2004**, *126*, 4228−4233.
(31) Fdez. Galván, I.; Sánchez, M. L.; Martín, M. E.; Olivares del Valle, F. J.; Aguilar, M. A. ASEP/MD: A program for the calculation of solvent effects combining QM/MM methods and the mean field approximation. *Comput. Phys. Commun.* **2003**, *155*, 244−259.
(32) García-Prieto, F. F.; Fdez. Galván, I.; Muñoz-Losa, A.; Aguilar, M. A.; Martín, M. E. Solvent effects on the absorption spectra of the para-coumaric acid chromophore in its different protonation forms. *J. Chem. Theory. Comput.* **2013**, *9*, 4481−4494.
(33) Wang, Y.; Li, H. Excited state geometry of photoactive yellow protein chromophore: A combined conductorlike polarizable continuum model and time-dependent density functional study. *J. Chem. Phys.* **2010**, *133*, 034108.
(34) Angyan, J. G. Common theoretical framework for quantum chemical solvent effect theories. *J. Math. Chem.* **1992**, *10*, 93−137.
(35) Tapia, O. In *Theoretical Models of Chemical Bonding, Part 4*, Maksic, Z. B., Ed.; Springer-Verlag: Berlin, 1991, 435.
(36) Warshel, A.; Levitt, M. Theoretical studies of enzymic reactions: Dielectric, electrostatic and steric stabilization of the carbonium ion in the reaction of lysozyme. *J. Mol. Biol.* **1976**, *103*, 227−249.
(37) Martín, M. E.; Sánchez, M. L.; Corchado, J. C.; Muñoz-Losa, A.; Fdez. Galván, I.; Olivares del Valle, F. J.; Aguilar, M. A. Theoretical study of the role of solvent stark effect in electron transitions. *Theor. Chem. Acc.* **2011**, *128*, 783−793.
(38) Coutinho, K.; Rivelino, R.; Georg, H. C.; Canuto, S. *Solvation Effects on Molecules and Biomolecules. Computational Methods and Applications*; Canuto, S., Ed.; Springer: New York, 2008.
(39) Allen, M. P.; Tildesley, D. J. *Computer Simulation of Liquids*; Oxford University Press: Oxford, 1987.
(40) Chirlian, L. E.; Francl, M. M. Atomic charges derived from electrostatic potentials: A detailed study. *J. Comput. Chem.* **1987**, *8*, 894−905.
(41) Breneman, M.; Wiberg, K. B. Determining atom-centered monopoles from molecular electrostatic potentials. The need for high sampling density in formamide conformational analysis. *J. Comput. Chem.* **1990**, *11*, 361−373.
(42) Ten-no, S.; Hirata, F.; Kato, S. A hybrid approach for the solvent effect on the electronic structure of a solute based on the RISM and Hartree-Fock equation. *Chem. Phys. Lett.* **1993**, *214*, 391−396.
(43) Sato, H.; Hirata, F.; Kato, S. Analytical energy gradient for the reference interaction site model multiconfigurational self-consistent-field method: application to 1,2-difluoroethylene in aqueous solution. *J. Chem. Phys.* **1996**, *105*, 1546.
(44) Hirata, F. *Molecular Theory of Solvation*, Hirata, F., Ed.; Kluwer Academic Publisher: Dordrecht, The Netherlands, 2004.
(45) Coutinho, K.; Georg, H. C.; Fonseca, T. L.; Ludwig, V.; Canuto, S. An efficient statistically converged average configuration for solvent effects. *Chem. Phys. Lett.* **2007**, *437*, 148−152.
(46) Nakano, H.; Yamamoto, T. Variational calculation of quantum mechanical/molecular mechanical free energy with electronic polarization of solvent. *J. Chem. Phys.* **2012**, *136*, 134107.
(47) Zhou, X.; Kaminski, J. W.; Wesolowski, T. A. Multi-scale modelling of solvatochromic shifts from frozen-density embedding theory with non-uniform continuum model of the solvent: The coumarin 153 case. *Phys. Chem. Chem. Phys.* **2011**, *13*, 10565−10576.
(48) Fdez. Galván, I.; Sánchez, M. L.; Martín, M. E.; Olivares del Valle, F. J.; Aguilar, M. A. Geometry optimization of molecules in solution: Joint use of the mean field approximation and the free energy gradient method. *J. Chem. Phys.* **2003**, *118*, 255−263.
(49) Okuyama-Yoshida, N.; Nagaoka, M.; Yamabe, T. Transition-state optimization on free energy surface: Toward solution chemical reaction ergodography. *Int. J. Quantum Chem.* **1998**, *70*, 95−103.
(50) Okuyama-Yoshida, N.; Kataoka, M.; Nagaoka, M.; Yamabe, T. Structure optimization via free energy gradient method: Application to glycine zwitterion in aqueous solution. *J. Chem. Phys.* **2000**, *113*, 3519.
(51) Hirao, H.; Nagae, Y.; Nagaoka, M. Transition-state optimization by the free energy gradient method: Application to aqueous-phase Menshutkin reaction between ammonia and methyl chloride. *Chem. Phys. Lett.* **2001**, *348*, 350−356.
(52) Zhang, Y.; Liu, H.; Yang, W. Free energy calculation on enzyme reactions with an efficient iterative procedure to determine minimum energy paths on a combined ab initio QM/MM potential energy surface. *J. Chem. Phys.* **2000**, *112*, 3483.
(53) Roos, B. O. *Ab Initio Methods in Quantum Chemistry*, Lawley, K. P., Ed.; Wiley: New York, 1987.
(54) Fdez. Galván, I.; Martín, M. E.; Aguilar, M. A.; Ruiz-López, M. F. Comparison of three effective Hamiltonian models of increasing complexity: Trizene in water as a test case. *J. Chem. Phys.* **2006**, *124*, 214504.
(55) Malmquist, P. A.; Roos, B. O. The CASSCF state interaction method. *Chem. Phys. Lett.* **1998**, *155*, 189−194.
(56) Andersson, K.; Malmquist, P.Å.; Roos, B. O. Second-order perturbation theory with a complete active space self-consistent field reference function. *J. Chem. Phys.* **1992**, *96*, 1218.
(57) Finley, J.; Malmquist, P. Å.; Roos, B. O.; Serrano, L. The multi-state CASPT2 method. *Chem. Phys. Lett.* **1998**, *288*, 299−306.

DOI: 10.1021/acs.jpca.5b01434
J. Phys. Chem. A 2015, 119, 5504−5514

(58) Berendsen, H. J. C.; van der Spoel, D.; van Drunen, R. GROMACS: A message-passing parallel molecular dynamics implementation. *Comput. Phys. Commun.* **1995**, *91*, 43−56.
(59) Lindahl, E.; Hess, B.; van der Spoel, D. GROMACS 3.0: A package for molecular simulation and trajectory analysis. *J. Mol. Model.* **2001**, *7*, 306−317.
(60) Aquilante, F.; De Vico, L.; Ferré, N.; Ghigo, G.; Malmqvist, P.-Å; Neogrády, P.; Pedersen, T. B.; Pitonak, M.; Reiher, M.; Roos, B. O.; et al. MOLCAS 7: The next generation. *J. Comput. Chem.* **2010**, *31*, 224−247.
(61) Jorgensen, W. L.; Maxwell, D. S.; Tirado-Rives, J. Development and testing of the OPLS All-Atom force field on conformational energetics and properties of organic liquids. *J. Am. Chem. Soc.* **1996**, *118*, 11225−11236.
(62) Jorgensen, W. J.; Madura, J. D. Temperature and size dependence for Monte Carlo simulation of TIP4P. *Mol. Phys.* **1985**, *56*, 1381−1392.
(63) Darden, T.; York, D.; Pedersen, L. Particle mesh Ewald: An N-log(N) method for Ewald sums in large systems. *J. Chem. Phys.* **1993**, *98*, 10089.
(64) Hoover, W. G. Canonical dynamics: Equilibrium phase-space distributions. *Phys. Rev. A* **1985**, *31*, 1695−1697.
(65) Muguruza González, E.; Guidoni, L.; Molteni, C. Chemical and protein shifts in the spectrum of the photoactive yellow protein: a time-dependent density functional theory/molecular mechanics study. *Phys. Chem. Chem. Phys.* **2009**, *11*, 4556−4563.
(66) Sergi, A.; Crüting, M.; Ferrario, M.; Buda, F. Density functional study of the photoactive yellow protein's chromophore. *J. Phys. Chem. B* **2001**, *105*, 4386−4391.
(67) Frutos-Puerto, S.; Muñoz-Losa, A.; Martín, M. E.; Aguilar, M. A. Theoretical study of the absorption and emision spectra of the anionic p-coumaric methyl ester in gas phase an in solution. *Comput. Theor. Chem.* **2014**, *1040−1041*, 287−294.
(68) Naseem, S.; Laurent, A. D.; Carroll, E. C.; Vengris, M.; Kumauchi, M.; Hoff, W. D.; Krylov, A. I.; Larsen, D. S. Photoisomerization upshifts the pK_a of the photoactive yellow protein chromophore to contribute to photocycle propagation. *J. Photochem. Photobiol., A* **2013**, *270*, 43−52.
(69) Larsen, D. S.; Vengris, M.; van Stokkum, I. H. M.; van der Horst, M. A.; Cordfunke, R. A.; Hellingwerf, K. J.; van Grondelle, R. Initial photo-induced dynamics of the photoactive yellow protein chromophore in solution. *Chem. Phys. Lett.* **2003**, *369*, 563−569.

DOI: 10.1021/acs.jpca.5b01434
J. Phys. Chem. A 2015, 119, 5504−5514